Letters

Intergranular precipitation in austenitic alloys

Various workers have attempted to predict theoretically the kinetics of grain boundary precipitation. Early work of Zener [1] was successfully developed by Aaron and Aaronson [2] and Brailsford and Aaron [3]. Aaron and Aaronson's model was most successful in relating theory to practice, particularly with aluminium alloys. More recently, Faulkner and Caisley [4] have refined the Aaron and Aaronson model for conditions specific to early stages of precipitation. This approach is successful in predicting intergranular precipitation of carbides in the high nickel alloy, Nimonic* PE16 (see Table I for composition).

This letter shows predicted behaviour for two other austenitic alloys; Alloy 800 and 20/25 Cr–Ni–Nb steel (see Table I for compositions). Experimental intergranular precipitation data have recently been reported [5, 6] for these two alloys. Favourable comparison of experimental results with theoretical predictions is shown, indicating that the model can be applied more generally to austenitic alloys.

A convenient way of presenting results on intergranular precipitation is by means of isothermal precipitation curves. These show the time taken for a given dimension of the grain boundary precipitate to reach a given size as a function of temperature. All models begin on the premise that the atom flux arriving at the edge of the precipitate is converted into new precipitate.

The flux arriving at the precipitate is given for the grain boundary situation by [2]:

$$\frac{dm}{dt} = \frac{A_v D^{1/2}}{\pi^{1/2}} (x_\alpha - x^{\alpha\theta}_{\alpha(r)}) \rho_s^{-\alpha} t^{-1/2} \quad (1)$$

where

A_v is the area of grain boundary associated with each precipitate

D is the volume diffusion coefficient for the solute in the matrix

x_α is the concentration of solute in the matrix (volume fraction)

$\rho_s^{-\alpha}$ is the partial molar density of the solute in the matrix

t is time

$x^{\alpha\theta}_{\alpha(r)}$ is the equilibrium concentration of solute in terms of volume fraction at the precipitate–matrix interface, corrected for the Gibbs–Thompson effect as given below

$$x^{\alpha\theta}_{\alpha(r)} = x^{\alpha\theta}_{\alpha} \exp\left(\frac{2\gamma\Omega}{RTr'}\right)$$

where

r' is the radius of curvature of the precipitate at the point where growth is taking place

Ω is the atomic volume of the solute in the matrix

γ is the interfacial energy between matrix and precipitate.

Details of the calculation of $x^{\alpha\theta}_{\alpha}$ are given in [4].

The growth of the precipitate fed by this flux is determined by the choice of growth form. Faulkner and Caisley [4] found that for early stages of growth of intergranular precipitates in Nimonic PE 16 matrices the precipitates can be imagined as small discs of constant aspect ratio. Under these circumstances the rate at which the thickness of the precipitate disc increases in terms of the arriving solute atom flux is given by ds/dt where [4]:

$$\frac{dm}{dt} = 3\pi k_1^2 s^2 (x_\theta - x^{\alpha\theta}_{\alpha(r)}) \rho_s^{-\alpha} \frac{ds}{dt} \quad (2)$$

where

k_1 is the aspect ratio

s is the precipitate thickness

x_θ is the concentration of solute in the precipitate (volume fraction)

Equating Expressions 1 and 2 and integrating with respect to s and t,

$$t = \frac{s^6 \pi^2 k_1^4 (x_\theta - x^{\alpha\theta}_{\alpha(r)})^2}{4 A_v D (x_\alpha - x^{\alpha\theta}_{\alpha(r)})^2} \quad (3)$$

The rate-determining step during growth is solute arrival at the precipitate (Equation 2) rather than atom transfer along the precipitate–matrix interface. Making this assumption theoretical isothermal precipitation curves are produced for Nimonic PE 16 which show good fits with experimentally observed data in the same alloy for

*Trade mark of Henry Wiggin & Co. Ltd.

0022–2461/79/092249–05 $02.50/0

TABLE I Compositions of alloys (wt%)

Alloy	Fe	Ni	Cr	Mo	Ti	Al	Nb	Mn	Si	C
Nimonic PE 16	bal.	42.5	17.1	3.1	1.2	1.3	–	0.05	–	0.08
Alloy 800	bal.	33.5	20.6	–	0.46	0.51	–	1.21	0.49	0.019
20/25 Cr–Ni–Nb Steel	bal.	25.0	20.0	–	–	–	0.52	–	–	0.049

carbides measuring 25 Å thickness by 100 Å diameter.

The times for nucleation have not as yet been considered in the model. At low temperatures ($<0.4\,T_m$) diffusion will be so slow that nucleation time could become significant [2]. Also near the precipitate solvus temperature nucleation rates are likely to decrease because of a lack of volume-free energy based driving force. However, nucleation rates will be at a maximum in the nose regions of the isothermal precipitation curves. These regions are those which are considered in most detail in this paper and therefore the use of a pure growth model is considered justified.

Volume concentrations are used throughout since the theory involves moving equal volumes of material from one point to another. Compensation for the partial molar volume effect is not necessary because the correction terms cancel in the derivation of Equation 3.

In this work theoretical isothermal precipitation curves for intergranular precipitates of disc shape with aspect ratio 4 and thickness 25 Å have been produced for two austenitic alloys using the above model (Equation 3).

Using data given in Table II, $M_{23}C_6$ and TiC precipitates have been considered for Alloy 800 (see Table I for composition) (Fig. 1) while $M_{23}C_6$ and NbC precipitates have been considered for 20/25: Cr–Ni–Nb steel (see Table I for composition) (Fig. 2). M represents a mixture of chromium and iron. The area of grain boundary associated with each precipitate (A_v) is assumed to be $2.25 \times 10^{-12}\,m^2$. In the Gibbs–Thompson correction r' is assumed to be 10^{-7}m and the atomic volume of the solute in the matrix (Ω) is assumed as $15 \times 10^{-6}\,m^3\ mol^{-1}$. Several theoretical curves are shown on Figs. 1 and 2 displaying the possible growth for a range of available carbon contents in the alloys.

The recent experimental data of Sanderson [5] for Alloy 800 and of Adamson [6] for 20/25 Cr–Ni–Nb steel are also plotted in Figs. 1 and 2. Both of these sets of data refer to $M_{23}C_6$.

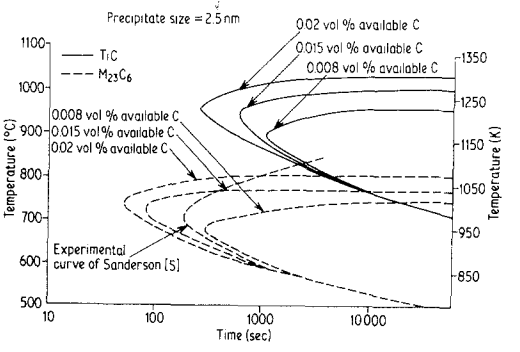

Figure 1 Isothermal precipitation curves for intergranular $M_{23}C_6$ and TiC in Alloy 800.

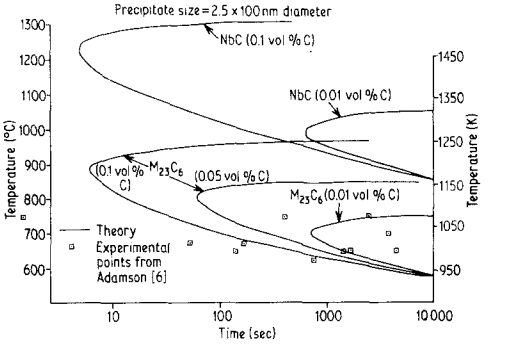

Figure 2 Theoretical isothermal precipitation curves for intergranular $M_{23}C_6$, and NbC in 20/25 chromium nickel–niobium steel.

The Adamson data are adapted from the quoted results [6]. Adamson states that the precipitates are spherical. The long dimension of the disc-shaped particles assumed in the theory is therefore taken as the sphere diameter measured experimentally. Furthermore, Adamson's data refer to particles 1000 Å in diameter. Since the Faulkner and Caisley approach is only intended to apply to early stages of growth, the times taken to grow the particles to 100 Å diameter are extrapolated from the quoted values. This is done using an expression given by Adamson to express the growth of par-

TABLE II Data for isothermal precipitation curves

Precipitate	x_α (volume fraction)	x_θ (volume fraction)	D ($m^2 sec^{-1} \times 10^{-4}$)	$x_\alpha^{\alpha\theta}$ (volume fraction)	C_c (volume fraction)	γ ($J\ m^{-2} \times 10^{-3}$)
20/25 Cr–Ni–Nb steel						
$M_{23}C_6$	0.224	0.84	$0.19 \exp(-58\,800/RT)$ [10]	$\left\{\frac{1}{C_c} \exp[(-28\,800/RT) - 0.9]\right\}^{6/23}$ [8]	0.0001 –0.001	300
NbC	0.0055	0.67	$530 \exp(-82\,300/RT)$ [11]	$\frac{1}{C_c} \exp[(-38\,400/RT) + 0.15]$ [12]	0.0001 –0.001	2000
Alloy 800						
$M_{23}C_6$	0.232	0.84	$0.15 \exp(-54\,900/RT)$ [4]	$\left\{\frac{1}{C_c} \exp[(-28\,800/RT) - 0.9]\right\}^{6/23}$ [8]	0.00008 –0.0002	300
TiC	0.0083	0.66	$0.15 \exp(-60\,000/RT)$ [13]	$\frac{1}{C_c} \exp[(-40\,500/RT) + 2.5]$ [14]	0.00008 –0002	2000

ticles on the grain boundaries in the temperature range of interest. This states that the time taken to grow a particle 1000 Å in diameter, t_{1000}, is given by

$$t_{1000} = \frac{10^6 t}{x^2} \quad (4)$$

where x is the particle radius measured at time t.

The choice of available carbon content for Alloy 800 is based on the following observations made by Sanderson [5]. There was more undissolved TiN than TiC and of the available TiC much was Ti(C,N). According to the optical microscope observations of Sanderson's alloy there are about 0.9 vol% of undissolved particles. If 20% of these are TiC or Ti(C,N) and there is three times the amount of Ti(C,N) compared with TiC, then 0.056 vol% carbon is associated with undissolved particles. Since there is 0.071 vol% carbon in the alloy, assuming a density of 8.6×10^3 kg m^{-3}, this leaves 0.015 vol% carbon available for further precipitation. Using this figure a reasonable fit between experiment and theory is obtained for $M_{23}C_6$ (Fig. 1). The constants used for $M_{23}C_6$ in Table II have been made assuming that M represents pure chromium. Although Da Casa [7] has shown that up to 30% iron can substitute for chromium in this compound, this is not thought likely to affect greatly the validity of the results. Furthermore, Sanderson reports that more intergranular TiC was seen in the material solution treated at 950° C compared to that solution-treated at 1050° C. This finding is supported by the predictions of Fig. 1 which suggest that all small particles of TiC should dissolve at temperatures above 1000° C for an alloy with 0.015 vol% available carbon.

The available carbon content in the 20/25 Cr–Ni–Nb steel is 0.17 vol%. For the same reasons as discussed in the previous paragraph over half of this carbon is probably connected with large, undissolved carbides or carbonitrides. No $M_{23}C_6$ is present at temperatures above 850° C in this alloy, which indicates the position of the solubility limit. As can be seen, this is the temperature predicted for the solubility limit for a 0.05 vol% available carbon content. Therefore, a 0.05 vol% carbon level is assumed to be most appropriate in this case. Fig. 2 shows that reasonable agreement is obtained between experimental points and the theoretical 0.05 vol% available carbon content curve for $M_{23}C_6$ in the alloy.

It should be emphasised that in positions away from the noses of the curves the precipitate behaviour may be incorrectly predicted. This is because the nucleation rates are lower in these regions and therefore allowance should be made for nucleation in the kinetics appraisal. In addition, in temperature zones where more than one carbide type is expected, there will be a sharing of available carbon between the two types of precipitates. Thus the predicted curves will overestimate the time needed to achieve a certain precipitate size. The important point to remember is that the positions of the noses of the curves are reasonably well placed and it is precisely these regions in which commercial heat treatment engineers are interested.

The effects of non-stoichiometric compositions in the alloys were not considered because, as was discussed in [4], the model only applies to the very early stages of precipitate growth. Therefore no consideration of events occurring when either solute or carbon supply to the precipitate ceases is necessary.

The niobium carbide curve is likely to be the most inaccurate of the curves for the three carbides considered. This is because there is some doubt as to the actual composition of the carbide. Deighton [8] has considered the solubility of NbC in austenitic matrices. However, there is some evidence that $NbC_{0.9}$ forms in low alloy and ferritic steels [9]. Deighton's data are thought to be most applicable in the cases of the alloys discussed here.

A theoretical model for grain boundary precipitate growth developed by Aaron and Aaronson with modifications for small, constant aspect ratio particles made by Faulkner and Caisley is discussed. The modified model is shown to give reasonably good fits between theory and experimental data for $M_{23}C_6$ and TiC intergranular precipitation in Alloy 800 and for $M_{23}C_6$ intergranular precipitation in 20/25 Cr–Ni–Nb steel.

Acknowledgements

Encouragement and support from Dr D. R. Harries and Dr S. J. Sanderson of the Metallurgy Division AERE, Harwell is gratefully acknowledged. Provision of laboratory and computing facilities at the University of Loughborough by Professor I.A. Menzies is appreciated.

References

1. C. ZENER, *J. Appl. Phys.* **20** (1949) 950.
2. H. B. AARON and H. I. AARONSON, *Acta Met.* **16** (1968) 789.
3. A. D. BRAILSFORD and H. B. AARON, *J. Appl. Phys.* **40** (1969) 1702.
4. R. G. FAULKNER and J. CAISLEY, *Metal Sci.* **11** (1977) 200.
5. S. J. SANDERSON, *ibid.* **11** (1977) 23.
6. J. P. ADAMSON, D. Phil. Thesis, University of Oxford (1972).
7. C. da CASA, V. B. NILESHWAR and D. A. MELFORD, *J. Iron and Steel Inst.* **207**. (1969) 1325.
8. M. DEIGHTON, *ibid.* **208** (1970) 1012.
9. B. AARONSON, Proceedings of the Conference on "Steel Strengthening Mechanisms" (Climax Molybdenum Co., Greenwich, Conn., 1969) p. 77.
10. A. F. SMITH and G. B. GIBBS, *Metal Sci. J.* **3** (1969) 93.
11. B. SPARKE, D. W. JAMES and G. M. LEAK, *J. Iron and Steel Inst.* **203** (1965) 152.
12. M. DEIGHTON, *ibid.* **205** (1967) 535.
13. S. H. MOLL and R. E. OGILVIE, *Trans. Met. Soc. AIME* **215** (1959) 613.
14. F. R. BECKETT and T. GLADMAN, BSC Research Report SSD 818 (1972).

Received 18 October 1978
and accepted 21 February 1979.

R. G. FAULKNER
Department of Materials Engineering and Design, University of Technology, Loughborough, Leicestershire, UK

Hot hardness of SiC single crystal

Silicon carbide (SiC) is one of the hardest and most refractory materials and is of considerable interest as a high-temperature structural material [1]. Hardness is an important factor in the choice of ceramics for abrasives, tool bits, bearings and wear resistant coatings, and it generally correlates with both micro- and macro-plastic deformation and with the ease of machining [2]. In the case of SiC, the room temperature hardness has been examined in some detail [3–6], whereas the knowledge of high-temperature hardness (hot hardness) is quite limited [7, 8]. Up to now no attempt has been made to analyse the hot hardness of SiC single crystals. In this work, the Vickers microhardness (VMH) tests were made on the basal plane and two kinds of prismatic planes ($\{1\,0\,\bar{1}\,0\}$ and $\{1\,1\,\bar{2}\,0\}$) of the single crystal of 6H-polytype SiC, from room temperature up to 1500° C. The creep behaviour at high temperatures was also investigated by hardness measurements at high temperatures.

6H-SiC single crystals were grown from melts of silicon, carbon and sodium chloride [9]. The planes for hardness tests were polished by various grades of diamond paste (3 to 0.25 μm). Hardness measurements were made using a high-temperature micro-hardness tester (Nikon, Model QM) in a vacuum of 1×10^{-5} to 5×10^{-4} Torr [10]. In almost all measurements, 100 g loads were applied for 10 sec at a lowering rate of 0.3 mm sec^{-1}. Loads of 25 to 500 g and loading times of 0.1 sec to 1 h were used for observations of the deformation behaviour around indentations and for creep tests, respectively. The VMH values reported in this work represent the average of at least 10 indentation measurements. The failure of diamond indenter's tip by chemical reaction, mechanical fracture and graphitization [11] was not observed.

Fig. 1 shows the temperature dependence of VMH at a 100 g load on (0 0 0 1), $\{1\,0\,\bar{1}\,0\}$ and $\{1\,1\,\bar{2}\,0\}$ planes a 6H-SiC single crystal. Measurements were performed when one of the indenter diagonals was aligned $\langle 1\,0\,\bar{1}\,0\rangle$ on the basal plane and [0 0 0 1] on the prismatic planes. The random errors in these measurements were considerably reduced with increasing temperature

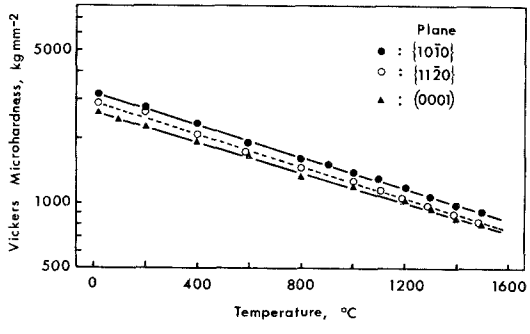

Figure 1 Temperature dependence of Vickers microhardness for the (0 0 0 1), $\{1\,0\,\bar{1}\,0\}$ and $\{1\,1\,\bar{2}\,0\}$ planes of 6H-SiC single crystal (100 g load).

